Available online at www.sciencedirect.com
ScienceDirect
Journal of Magnetic Resonance 183 (2006) 25–31
JMR Journal of Magnetic Resonance
www.elsevier.com/locate/jmr

A mobile one-sided NMR sensor with a homogeneous magnetic field: The NMR-MOLE

B. Manz [a,b,*], A. Coy [a], R. Dykstra [c], C.D. Eccles [a], M.W. Hunter [d], B.J. Parkinson [d], P.T. Callaghan [d]

[a] *Magritek Limited, 32 Salamanca Road, Wellington, New Zealand*
[b] *Arbeitsgruppe Magnetische Resonanz, Fraunhofer-Institut für Biomedizinische Technik, Ensheimer Straße 48, DE-66386 St. Ingbert, Germany*
[c] *Institute of Fundamental Sciences, Massey University, Palmerston North, New Zealand*
[d] *MacDiarmid Institute for Advanced Materials and Nanotechnology, Victoria University of Wellington, New Zealand*

Received 27 March 2006; revised 30 June 2006
Available online 7 August 2006

Abstract

A new portable NMR sensor with a novel one-sided access magnet design, termed NMR-MOLE (MObile Lateral Explorer), has been characterised in terms of sensitivity and depth penetration. The magnet has been designed to be portable and create a volume with a relatively homogeneous magnetic field, 15,000 ppm over a region from 4 to 16 mm away from the probe, with maximum sensitivity at a depth of 10 mm. The proton NMR frequency is 3.3 MHz. We have demonstrated that with this approach a highly sensitive, portable, unilateral NMR sensor can be built. Such a design is especially suited for the characterisation of liquids in situations where unilateral or portable access is required.

Keywords: Unilateral NMR; T_2 relaxation; One-sided access magnet; Rf coil; NMR-MOLE

1. Introduction

Portable one-sided access (OSA) nuclear magnetic resonance probes have been built and used successfully by several groups. These probes can be categorised into two classes: The first group operates in a strong magnetic field gradient [1–3], whereas the second uses a region of more or less homogeneous fields [4–11]. Both approaches have their strengths and weaknesses. This paper demonstrates a complete OSA NMR system based on the second class, and more specifically akin to that proposed by Fukushima and Jackson [4]. The focus here is on the overall system design and performance.

In order to create a volume with a uniform magnetic field at some distance from the magnet, it is necessary to tailor the field in a special way, typically using overlapping fields from several coils or permanent magnets [4]. This makes the whole magnet arrangement bulkier and results in weaker polarising fields than in the case of magnet systems which tolerate field gradients, where in the simplest case one bar magnet is sufficient [1]. However, the measurement of a NMR signal in a strong magnetic field gradient results in a very broad frequency spectrum, which reduces the signal-to-noise ratio. This breadth requires the rf pulses to be very short, with high consequent power, in order to achieve the desired frequency bandwidth. Liquids with fast diffusion can usually not be characterised with such probes, because of the fast signal decay in the magnetic field gradient. The second class of probes therefore has a significant advantage in measuring the true T_2 of liquids.

For the measurement of liquid or moisture content more than a few millimetres inside a sample the second class of probes is more suitable. Although for this class the polarising field, and therefore sensitivity, is smaller than if using a gradient, this loss is compensated by an increased sensitive

* Corresponding author. Fax: +49 6894 980 400.
E-mail address: bertram.manz@ibmt.fraunhofer.de (B. Manz).

1090-7807/$ - see front matter © 2006 Elsevier Inc. All rights reserved.
doi:10.1016/j.jmr.2006.07.017

volume and by less diffusive attenuation. Furthermore, the frequency spectrum is very narrow compared to the first class of probes and this enables an additional enhancement of signal-to-noise ratio via appropriate bandpass signal filtering. One important source of external noise in OSA NMR is the occurrence of frequency spikes due to radio signals or other electronic equipment. For a spectrum with a width of a few tens of kHz it is relatively easy to find a gap in the noise spectrum, compared to a broad spectrum with a width of hundreds of kHz, making this second class of probes less susceptible to external noise.

In this paper we report first experiments on a portable NMR probe termed NMR-MOLE, which is based on a novel OSA magnet design [12]. NMR-MOLE stands for MObile Lateral Explorer, with the name gaining inspiration from the NMR-MOUSE, but with the feature that the MOLE works with a much lower magnetic field gradient, making it easier to sample proton NMR signals from liquid state molecules. The term MOLE can also stand for MObile Liquid Explorer to reflect this capability. The ability to characterise liquids will be demonstrated in this paper, and as an example for possible applications we will monitor the curing process of fresh cement paste. This shows that the NMR-MOLE could become a useful tool for applications where it is important to measure moisture content of large, immovable samples, such as a layer of poured concrete on a building site, or other liquids in large containers.

Fig. 1. (a) A schematic drawing of the bar magnet arrangement used to create a homogeneous magnetic field in a region outside the array. The ring magnets are spaced equally on a circle, with a further bar magnet positioned on the central axis. (b) A photograph of the assembled magnet array with optimised field homogeneity. See text for details.

2. Magnet design

The magnet array is based on a barrel magnet with a central magnet positioned to provide a region of homogeneity [4]. Our array shown in Fig. 1(a) uses a set of discrete magnets spaced equally on a circle, tilted by an angle alpha to the normal of the ring plane. Adjusting the angle alpha gives the opportunity to alter the position or the strength of the homogenous region [12]. The size of the homogenous region can further be increased by choosing appropriate dimensions of the central magnet [13]. Using discrete magnets instead of a continuous ring provides an inexpensive solution when using an angled array, although a compromise is made on field strength.

Given a practical rf bandwidth of 50 kHz a magnet array was designed to give a homogenous field of 76.7 mT centred at 15 mm from the array surface. To keep the dimensions of the magnet array a practical size and allowing a reasonable distance between the magnets, an array of 8 magnets was placed on a radius of 58.4 mm inclined at an angle of 11.5°. The diameter of the magnet array was 162 mm. The homogenous region was, in approximation, a sphere of diameter 20 mm, although the volume that contributes to the overall signal will depend on the sensitivity of the rf coil.

The magnet array consisted of cylindrical bar magnets (Macmill International, Nigbo, China) with length 50 mm, diameter 36 mm and a residual induction of approximately 1.3 T. These magnets were placed inside a Perspex block, which had been fitted with matching holes to produce a firm fit for the magnets. A central magnet of diameter 44 mm and length 4.5 mm was chosen to achieve the desired homogeneity. For the magnetic field calculations, the bar magnets were modelled as uniform, cylindrical current distributions. The calculations were performed in MATLAB using the Biot–Savart law [14].

The magnetic field of the assembled array was measured using a Gaussmeter (Lake Shore Cryotonics Inc., Westerville, Ohio). Its probe was attached to a home-built, computer controlled three-axis positioning device. Fig. 2 shows a two-dimensional field map of the optimised magnet array, both calculated (a) and measured (b). The maps compare well, considering the variation in residual induction of real magnets. The measured field plots show the homogenous region as an oblate spheroid with an equatorial diameter of around 23 mm and a polar diameter of around 11 mm. This will be the region for which the rf coil will be designed in the next section. With the housing and rf coils the homogeneous region was 10 mm from the surface of the assembly. The assembled probe, weighing 6 kg and with a total diameter of 200 mm, is shown in Fig. 1(b).

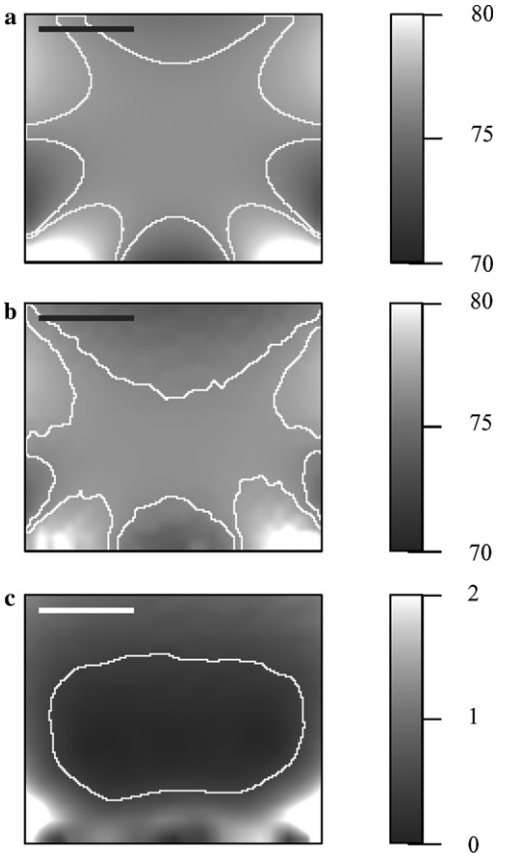

Fig. 2. The calculated (a) and measured (b) two-dimensional maps of the axial magnetic field strength B_z (given in mT) are shown for the magnet array displayed in Fig. 1(b). The orientation of the maps is such that the vertical direction is along the array axis, and the horizontal direction is parallel to its surface, with the lower end of the maps corresponding to the top surface of the magnet array. The white contour lines mark the boundary of the region where the Larmor frequency is within the 50 kHz bandwidth of the rf coil. (c) A map of the magnetic field gradient g (in T m^{-1}) is shown for the same orientation, with the contour line marking the $g = 0.2$ T m^{-1} boundary. The length of the scale bar is 10 mm in all images.

Although the 50 kHz frequency range (15,000 ppm over the sensitive volume) does not enable any chemical shift resolution on protons, it is still possible to characterise liquid samples through a measurement of the transverse relaxation time T_2, provided that the magnetic field gradient $g = |\mathrm{grad}(|\mathbf{B}|)|$ does not cause significant diffusive attenuation. In a spin-echo experiment with echo time T_e, the signal attenuation $E(T_e)$ of a liquid with diffusion coefficient D_s is given by

$$E(T_e) = R(T_e)D(T_e), \tag{1}$$

where the relaxation term is $R(T_e) = \exp(-T_e/T_2)$, and the diffusion term $D(T_e) = \exp(-2/3\gamma^2 g^2 T_e^3 D_s)$ [15]. For a typical liquid with $T_2 = 2$ s and $D_s = 2 \times 10^{-9}$ m^2 s^{-1}, it is easy to show that the diffusion term starts to dominate if $g > 0.2$ T m^{-1} for an echo time of 0.5 ms or larger. For such a liquid, the sensitive volume is then given by the region of the specified frequency range, and where $g \leqslant 0.2$ T m^{-1}. Fig. 2(c) shows a two-dimensional map of the magnetic field gradient along with the $g = 0.2$ T m^{-1} contour line. From the three-dimensional field map we find this volume to be 6200 mm^3, which roughly corresponds to a cylinder with a height of 10 mm and a diameter of 28 mm.

3. RF coil design

Particular care was taken with the design of the rf coil, because the sensitivity of the NMR method critically depends on its performance. As described above, the magnet array produces a homogeneous polarising field B_z orthogonal to the array surface. Therefore, the rf coil needs to create a magnetic field B_x parallel to the surface, a field which can be achieved using a so-called figure-eight meander coil [16], which consists of two bundles of parallel wires of length L. They are separated by a distance d, with straight return paths to each side of the bundle as shown in Fig. 3(a). The magnetic field above the centre of two parallel wires carrying the current I can be calculated using the law of Biot–Savart [14]:

$$B_x(x,0,z) = \frac{\mu_0 I}{2\pi} Lz \left(\frac{1}{R_-^2\sqrt{L^2+4R_-^2}} + \frac{1}{R_+^2\sqrt{L^2+4R_+^2}} \right), \tag{2}$$

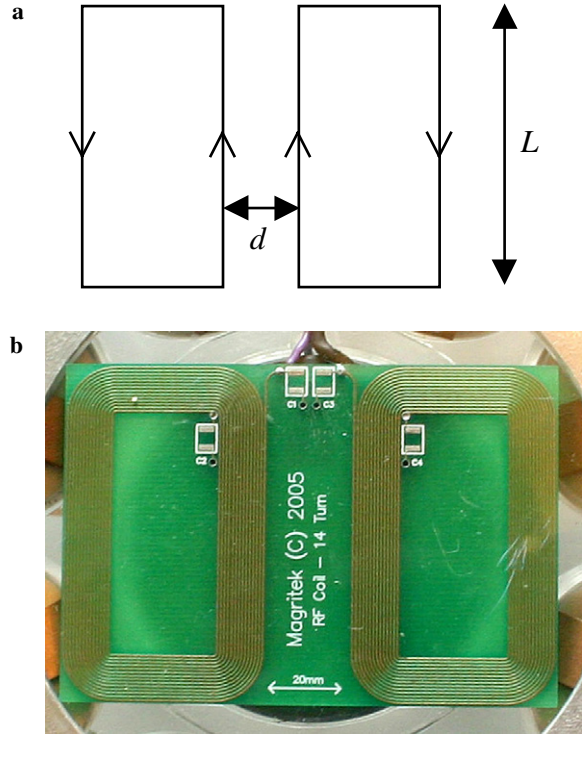

Fig. 3. (a) A schematic drawing of the figure-eight coil. It consists of two parallel wires with length L. They are separated by a distance d, with straight return paths to each side of the central legs. The current direction is indicated by arrows. (b) Photograph of a 14-turn figure-eight coil with $d = 20$ mm manufactured on PCB. The size of the board is 72 mm × 50 mm.

where $R_- = \sqrt{z^2 + (x - d/2)^2}$ and $R_+ = \sqrt{z^2 + (x + d/2)^2}$ are the distances of the point to each of the two wires. Figs. 4(a) and (b) shows B_x for different values of d along the lines $x = 0$ and $z = 10$ mm, respectively. It is evident from the curves and Eq. (2) that the overall field strength decreases along the central line with increasing d. This decrease in field strength is traded against an increase in field homogeneity (and thus sensitive rf volume), as the position of the field maximum increases. It is therefore necessary to find a suitable compromise between the required field strength and field homogeneity in the region of homogeneous polarising field, taking account of the return legs and a finite number of turns. Because the direction of the current in the return legs is opposite to the central wires, the return legs will lead to an overall reduction in magnetic field strength in the region of interest. In order to keep this reduction small, the return legs should be as distant as possible from the central wires. The geometry of the magnet array restricts the separation of the return legs to a maximum of 70 mm. At this distance, the return legs reduce the strength of the rf field by approximately 10% in the region of interest, with no significant change in field homogeneity (cf. Fig. 4).

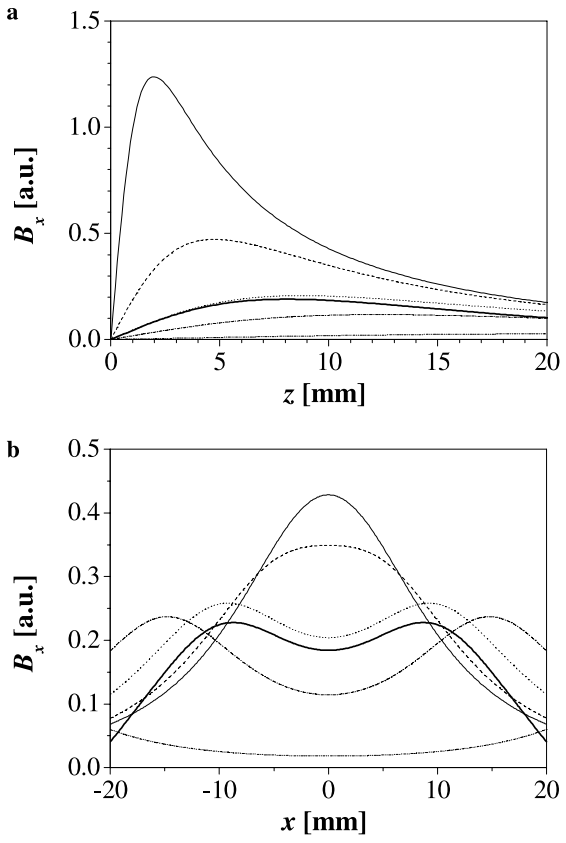

Fig. 4. The calculated magnetic field strength B_x of a figure-eight coil as a function of z above the centre of the coil (a), and as a function of x at a distance of 10 mm above the coil (b). The field strength is shown for $d = 4$ mm (—), 10 mm (- - -), 20 mm (· · ·), 30 mm (-·-·-) and 70 mm (-··-··-). The calculated field strength of the coil shown in Fig. 3(b) is shown as a solid bold line (—).

The coil sensitivity can be increased by increasing the number of turns, which results in a spiral-like rectangular pattern for the figure-eight coil. In order to calculate the effect of a finite number of turns on the field profile, the configuration with the best homogeneity ($d = 20$ mm) was compared to a configuration of two bundles of 14 parallel wires, with a separation of 0.5 mm between neighbouring wires and a bundle separation of 20 mm. The difference between both configurations is less than 3% in the region of interest, showing that the calculations using a single turn are a very good approximation.

Planar coils can be manufactured easily and very accurately on printed circuit board (PCB). A number of prototype figure-eight coils with different numbers of turns and bundle separations ranging between 8 and 33 mm was manufactured and tested. In the end it turned out that a 14-turn coil with $d = 20$ mm showed best overall performance on the magnet array, confirming the results of the calculations. The calculated magnetic field strength of this coil, normalised by the number of turns and including the return legs, is displayed in Fig. 4.

This coil (shown in Fig. 3(b)) was tuned to the resonance frequency of 3.27 MHz by connecting a number of fixed non-magnetic chip capacitors (ATC, Huntington Station, NY) to form a balanced tank circuit [17]. This circuit contains tuning capacitors of equal size on both sides of the coil in order to reduce the dielectric coupling to the sample, which leads to improved sensitivity compared to a standard circuit.

The specific values of the tuning and matching capacitors C_t and C_m not only determine the resonance frequency ν_0 of the circuit, but also its bandwidth $\Delta\nu$ and the quality factor $Q = \nu_0/\Delta\nu$, which in turn enters the signal-to-noise ratio as $Q^{1/2}$. Therefore, in terms of signal strength, a high Q is desired. But in practice there is an upper limit for Q, because the pulse ringdown time of the coil scales with Q/ν_0 [16]. For the liquid state applications considered here, circuit dead times of under 100 μs are acceptable. With the values of $C_t = 58$ pF and $C_m = 60$ pF we obtain $Q = 65$ and a pulse ringdown time of 60 μs. Above and in Fig. 2 we pointed out that the resulting frequency range of 50 kHz covers a large part of the homogeneous polarising field volume. In a perfectly homogeneous field, an increase in Q would in theory result in a signal increase by a factor of $Q^{1/2}$. But due to the frequency spread of the sample in a slightly inhomogeneous field, a higher value of Q will reduce the frequency bandwidth and therefore the excitation volume, which will result in a net signal loss.

4. Experimental

All experiments were performed at magritek using a Kea spectrometer (magritek Limited, Wellington, New Zealand). Unless stated otherwise, a large bottle of tap water was used as a sample. All initial adjustments were carried out using a spin-echo pulse sequence with echo time $\tau = 1$ ms. For the concrete experiment a bag of Portland

type GP cement (Golden Bay Cement, New Zealand) was obtained from a local hardware shop. Two pastes with different water cement ratios were made up by mixing 75 g cement with the appropriate amount of tap water (30 g and 45 g, respectively). The samples were stirred for 1 min and then transferred to the magnet. The signal was measured at room temperature every 10 min over a period of 20 h using a CPMG sequence with $T_e = 0.5$ ms. The repetition time was 2 s, which was long enough for the spins to recover, and the signal was averaged over 64 transients. For each experiment 64 echoes were acquired with subsequent Fourier transform and magnitude calculation. The intensities I_0 and T_2 values were calculated by performing a least-squared fit to the peak area with a single exponential fit function. After 20 h, the samples were weighed again to record the loss of moisture, which was below 10% of the original water content over that period.

5. Results and discussion

In order to perform spin-echo and CPMG experiments, it is essential to adjust the 180° pulse length for a given transmitter power. This was done by measuring the signal strength resulting from a T_p–τ–$2T_p$–τ spin-echo pulse sequence, where T_p denotes a rf pulse of duration T_p. Fig. 5(a) shows the integral of the phased spectrum with increasing pulse duration for two transmitter powers. Although a simple surface coil cannot be expected to produce a homogeneous rf field over a large sensitive region, a clear oscillation in the signal intensity can be recognised, the zero crossings corresponding to multiples of 180° pulses. It can also be noticed that the peak amplitude decreases as the pulse duration increases. There are two reasons for this behaviour: First, the phase spread across the sensitive volume increases due to rf inhomogeneities, causing the spectrum to become distorted. The second reason for a decrease in overall signal intensity with increasing pulse duration is the reduced spectral bandwidth, as discussed earlier.

A spin-echo spectrum with optimised pulse durations was recorded in order to characterise the sensitivity. Fig. 5(b) shows the spectrum of the sample and the empty probe using 8 signal averages, yielding a frequency domain signal-to-noise ratio of 27 per single scan. The full line width of the spectrum is approximately 50 kHz (corresponding

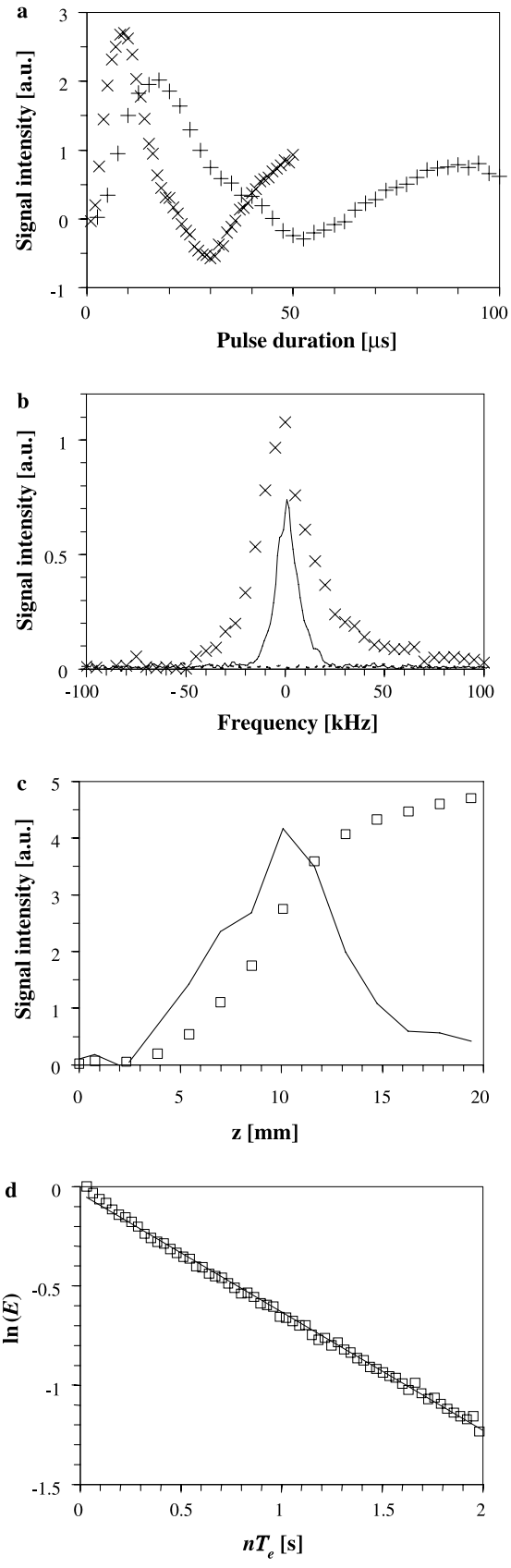

Fig. 5. (a) The integral of the phased spectrum with increasing pulse duration for a transmitter power of 50 W (+) and 150 W (×). The pulse duration where the first maximum occurs denotes the 90° pulse length. (b) Spectrum of a large water sample (solid line) and empty probe (dashed line) with 8 signal averages. The full line width of this spectrum is approximately 40 kHz and reflects the frequency bandwidth of the rf pulse. To avoid this frequency selection and measure the true frequency spread, the integrated intensity of a spectrum recorded at a series of different excitation frequencies is shown as symbols. (c) Signal intensity as a function of sample thickness (symbols), and sensitivity (solid line) as a function of distance from the probe surface. (d) CPMG echo signal decay from a large water sample with echo time $T_e = 0.5$ ms. The measured data points are shown as symbols, and the line represents a monoexponential curve fit with $T_2 = 1.7$ s. Note that the signal decay deviates slightly from a monoexponential decay due to diffusive attenuation. See text for details.

to 15,000 ppm), which is too broad to resolve any chemical shift on protons. However, it does not reflect the true frequency spread in the sensitive volume either, because its width is limited by the bandwidth of the rf pulses. In order to obtain the frequency distribution of the sample in the sensitive volume, which is not limited by the rf bandwidth, a series of 41 spectra was recorded with excitation frequencies ranging between 3.17 and 3.37 MHz. The integrated intensity of each spectrum is plotted as discrete points in Fig. 5(b). The half-width of this spectrum is around 30 kHz with a wide base, which is consistent with our previous estimates about the field distribution in the magnet array and the frequency range of the tank circuit. Of course a small sample positioned in the centre of the sensitive volume should produce a much narrower line. This has been confirmed experimentally, down to a linewidth of 1.5 kHz for a water sample with a cubic volume of $(4\ \text{mm})^3$ (data not shown).

In order to measure the depth of the sensitive volume, a profile was measured by recording the spin-echo signal intensity of a stack of soft rubber sheets. Each sheet had a thickness of 1.55 mm. Fig. 5(c) shows the signal intensity as a function of stack height, starting from the probe surface, as well as the increase in signal between subsequent measurements. The sensitive region extends from 4 to 16 mm above the surface of the magnet array, with maximum sensitivity at 10 mm away from the probe surface.

The inability of this system to resolve chemical shift means that different ways of characterising samples had to be explored with the NMR-MOLE. It has been shown that the spectrum of relaxation times or of self-diffusion coefficients can yield a lot of information about the molecular mobility in the sample, which can then be used for characterisation [18–21]. A fast and simple way to measure the transverse relaxation time T_2 is to acquire a number of spin-echoes in a CPMG train with pulse spacing τ [22,23]. Water has a fairly large T_2 value of several seconds, depending on the amount of dissolved oxygen and minerals. The echo signal is expected to decay mono-exponentially with increasing time. Fig. 5(d) shows the peak area of the spectrum of a large water sample for a CPMG experiment with echo time $T_e = 0.5$ ms, along with a mono-exponential fit line. The slight deviation from the mono-exponential decay suggests that background gradients cause an additional diffusive attenuation. This is in agreement with our calculations following Eq. (1) and gives us an estimate of the range of relaxation time values that can be measured accurately. A fit of these data yields an effective relaxation time T_2', which is weighted by diffusion as well as relaxation. From the experimental data we obtain a value of $T_2' = 1.7$ s, a limit above which diffusion starts to dominate signal decay of the CPMG experiment with $T_e = 0.5$ ms. In other words, the signal decay will be dominated by relaxation instead of diffusion, as long as the sample's largest T_2 value is below 1.7 s.

Having demonstrated the capability of the NMR-MOLE to perform basic NMR experiments, we will now show an application where both the portability and one-sided access are important. The curing process of wet concrete is very complex, involving several timescales [24–26]. Concrete is a composite material made up from a filler and a binder. The binder is usually a cement paste, which glues the particles of the filler together. It is the properties of this cement paste which controls the properties of the concrete. During the hydration process and the first few hours of curing, the water content of the mixture hardly changes, but the chemical reaction reduces the mobility of the water molecules. This should be reflected in the T_2 values of the water.

Fig. 6(a) shows the measured values of T_2 and I_0 for both cement paste samples. The sample with the higher water content gives a larger overall signal with higher T_2 values, but the time evolution is similar for both samples. In order to enhance the rate of change in T_2 values, the absolute value of the derivative is displayed in Fig. 6(b). A total of four stages of the hydration and curing process can be distinguished. The first stage occurs within 15 min after the addition of water and is characterised by fairly high T_2 values, which reflects free water in the sample. During the so-called dormancy period, the paste is in a plastic state which allows the concrete to be transported and placed without major difficulty. This stage II lasts for about 1–2 h, and the T_2 values are fairly constant during that period. For the next 5–6 h (stage III), the paste starts to

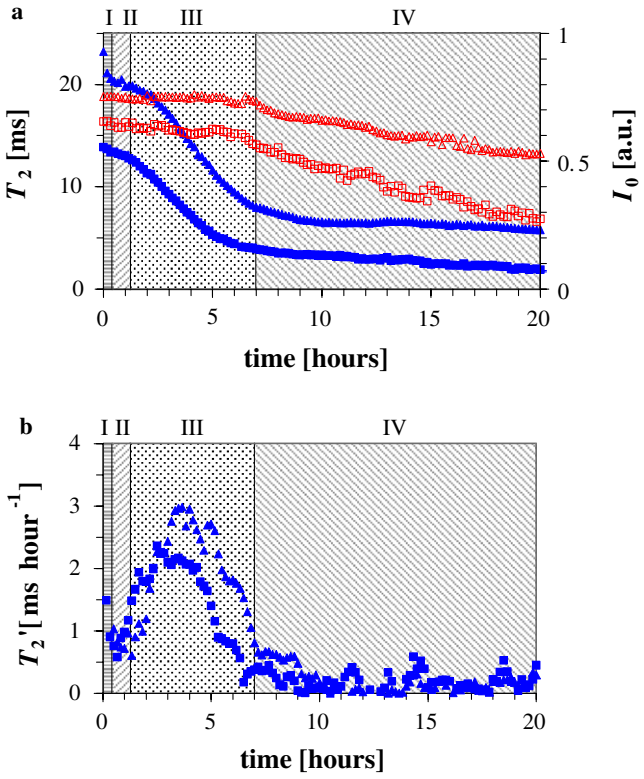

Fig. 6. (a) The measured values of T_2 (filled symbols) and I_0 (open symbols) for two cement paste samples with water/cement ratio 0.4 (squares) and 0.6 (triangles). The four stages of hydration are marked by differently shaded areas. (b) The rate of change in T_2 values for both samples.

harden due to chemical bonding of water molecules to calcium silicates, which is reflected in a dramatic drop in T_2. The signal intensity I_0 is constant during these first three stages, but starts to decrease with a steady rate at the same time as the rate of change in T_2 slows down. This marks the end of stage III and the beginning of stage IV. All these results are consistent with a recently published and extensive NMR diffusion and relaxation study on cement hydration [27]. As mentioned above, the loss of water due to evaporation is less than 10%, which is much smaller than the measured loss of NMR signal intensity. These unaccounted water molecules, which are still in the sample, but invisible with NMR, are those that have undergone tight chemical bonds to form crystals in the curing paste. The remaining signal can therefore be used as a measure for the wetness of the paste.

6. Conclusions

The use of a relatively homogeneous magnetic field in one-sided-access NMR proves remarkably effective in the examination of liquid state samples. For water samples, standard one-sided access probes [1,2], incorporating strong magnetic field gradients on the order of $10\ \mathrm{T\ m^{-1}}$, will experience significant signal attenuation inconsistent with the actual T_2, even for the shortest practical CPMG pulse spacing. For example with a pulse spacing of 0.1 ms, the effective T_2' of water under $10\ \mathrm{T\ m^{-1}}$ is 10 ms. By contrast, our magnet system has a volume of $6200\ \mathrm{mm^3}$ within a contour of $G = 0.2\ \mathrm{T\ m^{-1}}$ and unperturbed water signals may be easily observed.

Even allowing for the reduced B_0 field consequent on designing a region of field uniformity, the large homogeneous field sample volume allows for a superior signal-to-noise ratio performance, albeit at the expense of some loss of spatial resolution associated with the larger sensitive volume. We would argue however, that where one simply wishes to achieve maximum sensitivity from an extended sample at a distance on the order of 5 mm or greater from the probe surface, then the homogeneous field class of OSA probes provides the optimal solution.

Acknowledgment

The authors are grateful to the New Zealand Foundation for Research, Science and Technology for grant support.

References

[1] B. Blümich, V. Anferov, S. Anferova, M. Klein, R. Fechete, M. Adams, F. Casanova, Simple NMR-mouse with a bar magnet, Conc. Mag. Resonance B (Magn. Reson. Eng.) 15 (4) (2002) 255–261.
[2] G. Eidmann, R. Savelsberg, P. Blümler, B. Blümich, The NMR MOUSE, a Mobile Universal Surface Explorer, J. Magn. Reson. A 122 (1996) 104–109.
[3] P.J. Prado, Single sided imaging sensor, Mag. Reson. Imag. 21 (3–4) (2003) 397–400.
[4] E. Fukushima, J.A. Jackson, Unilateral magnet having a remote uniform field region for nuclear magnetic resonance, U.S. Patent No. 6,828,892, 2004.
[5] R.L. Kleinberg, A. Sezginer, D.D. Griffen, M. Fukuhara, Novel NMR apparatus for investigating an external sample, J. Magn. Reson. 97 (1992) 466–485.
[6] A.E. Marble, I.V. Mastikhin, B.G. Colpitts, B.J. Balcom, An analytical methodology for magnetic field control in unilateral NMR, J. Magn. Reson. 78 (2005) 78–87.
[7] E.A. Purea, Feasibility of Unilateral Nuclear Magnetic Resonance, MS thesis, Department of Physics, University of New Mexico, 2001.
[8] R. Kemmer, Coil-design for unilateral NMR with the barrel magnet, New Mexico Resonance Report, 2002.
[9] S. Utsuzawa, R. Kemmer, Y. Nakashima, K. Kose, Unilateral NMR apparatus using a novel barrel magnet, in: 46th Experimental NMR Conference, Providence, RI, April 10–15, 2005.
[10] S. Utsuzawa, R. Kemmer, Y. Nakashima, Unilateral NMR system by using a novel barrel shaped magnet, in: 8th International Conference on Magnetic Resonance Microscopy, Mibu, Japan, August 22–26, 2005.
[11] E. Fukushima, A concentric barrel-type magnet assembly for unilateral NMR, in: 8th International Conference on Magnetic Resonance Microscopy, Mibu, Japan, August 22–26, 2005.
[12] P.T. Callaghan, R. Dykstra, C.D. Eccles, M.W. Hunter, NMR Apparatus. International Patent No. PCT/NZ03/00149, New Zealand Patent Application 520114, 2002.
[13] M.W. Hunter, P.T. Callaghan, R. Dykstra, C.D. Eccles, S. Vamanan, Design and construction of a portable one-sided access NMR probe, Magn. Reson. Imag. 23 (2005) 407–444, P3.
[14] J.D. Jackson, Classical Electrodynamics, John Wiley and Sons, New York, 1962.
[15] P.T. Callaghan, Principles of Nuclear Magnetic Resonance Microscopy, Clarendon Press, Oxford, 1991.
[16] S. Anferova, V. Anferov, M. Adams, P. Blümler, N. Routley, K. Hailu, K. Kupferschläger, M.J.D. Mallett, G. Schroeder, S. Sharma, B. Blümich, Construction on a NMR-MOUSE with short dead time, Conc. Mag. Resonance (Magn. Reson. Eng.) 15 (2002) 15–25.
[17] J. Murphy-Boesch, A.P. Koretsky, An in vivo NMR probe circuit for improved sensitivity, J. Magn. Reson. 54 (1983) 526–532.
[18] S. Godefroy, P.T. Callghan, 2D relaxation/diffusion correlations in porous media, Magn. Reson. Imag. 21 (2003) 381–383.
[19] M.D. Hürlimann, M. Flaum, L. Venkataramanan, C. Flaum, R. Freedman, G.J. Hirasaki, Diffusion–relaxation distribution functions of sedimentary rocks in different saturation states, Magn. Reson. Imaging 21 (2003) 305–310.
[20] P.T. Callaghan, S. Godefroy, B.N. Ryland, Diffusion–relaxation correlation in simple pore structures, J. Magn. Reson. 162 (2003) 320–327.
[21] M.D. Hürlimann, L. Venkataramanan, Quantitative measurement of two-dimensional distribution functions of diffusion and relaxation in grossly inhomogeneous fields, J. Magn. Reson. 147 (2002) 31–42.
[22] H.Y. Carr, E.M. Purcell, Effects of diffusion of free precession in nuclear magnetic resonance experiments, Phys. Rev. 94 (3) (1954) 630–638.
[23] S. Meiboom, D. Gill, Modified spin-echo method for measuring nuclear relaxation times, Rev. Sci. Instrum. 29 (1958) 688–691.
[24] S. Abercrombie, Ferrocement: Building with Cement, Sand, and Wire Mesh, Schocken Books, New York, 1977.
[25] G.C. Bye, Portland Cement: Composition, Production and Properites, Pergamon Press, New York, 1983.
[26] S.H. Kosmata, W.C. Panarese, Design and Control of Concrete Mixtures, Portland Cement Association, 1988.
[27] K. Friedemann, F. Stallmach, J. Kärger, NMR diffusion and relaxation studies during cement hydration-A non-destructive approach for clarification of the mechanism of internal post curing of cementitious materials, Cement Concr. Res. 36 (2006) 817–826.